Separation of propeller-like particles by shear and electric field

M. Makino[1] and M. Doi[2]
[1]*Department of Mechanical Systems Engineering, Yamagata University, 4-3-16 Jonan, Yonezawa, Yamagata 992-8510, Japan*
[2]*Center of Soft Matter Physics and Its Applications, Beihang University, 37 Xueyuan Road, Haidian District, Beijing 100191, China*
(Received 27 December 2016; published 29 June 2017)

Separation of one type of chiral particle from mirror-image particles in a racemic mixture by shear flow and rotating electric field is studied theoretically. In shear flow the chiral particles and their mirror-image particles migrate in opposite directions along the vorticity direction. In a rotating electric field, they migrate in opposite directions along the axis of rotation. In each case, the migration velocity of the particles is calculated for a model chiral particle: a propeller-like particle which consists of two disks, at an angle to each other, rigidly connected to a thin rod. Effects of shear rate, field strength, and particle structure on the migration velocity are discussed. It is shown that the chirality of the particle is characterized by different parameters depending on the method of separation.

DOI: 10.1103/PhysRevFluids.2.064303

I. INTRODUCTION

A chiral particle is a particle whose mirror image cannot be superimposed on it by rotation. Separating one type of particle (R type) in the racemic mixture of the particles from its mirror-image particles (L type) is a scientific challenge which has potential applications in various fields of science and technology [1,2].

Conventional separation methods are based on crystallization which gives R-type crystals and L-type crystals, or on adsorption using the different permeability of R-type and L-type particles. In such methods, considerable efforts are needed as these techniques require the optimization of the crystallization conditions or the development of new filters for individual particles or molecules. Such methods have been developed for small molecules but have not been developed for large particles of size greater than 0.1 μm. For such large particles, other simpler methods which do not rely on the individual properties of the particles are needed. Two methods have been proposed for this purpose.

One method is to use the shear flow. It has been shown that chiral particles placed in a shear flow can have a nonzero average velocity along the vorticity direction [2,3]. Due to the physical law of mirror symmetry, if one type of chiral particle moves along the vorticity direction, the mirror-image type moves in the opposite direction, allowing for the separation of both types of particles.

The other method is to use a rotating electric field. If the particles are rotated by an external electric field, the chiral particles and the mirror-image particles migrate in opposite directions [4–6].

Though such separation can be shown to be possible using the argument of mirror symmetry, calculation of the actual migration velocity is not easy since one has to deal with the motion of particles which have a complex structure and are subject to Brownian motion. Accordingly, previous studies have been limited to the demonstration of the method [4–6]. Few studies have been reported on the relation between the migration velocity and the parameters characterizing the fields or the particle structures. In our previous works [3,6], we have studied the migration velocity of a chiral particle (a twisted ribbon) placed in shear flow [3] and in a rotating electric field [6]. However, the question of how the migration velocity is related to the chirality of the particle has not been discussed in detail. Chiral structure is generally characterized by a parameter called the chiral parameter [1], which is zero for a nonchiral particle, but is nonzero for a chiral particle. In this paper we consider a special type of chiral particle, a propeller-like particle (shown in Fig. 1), and discuss the relation between the migration velocity and the chiral parameter.

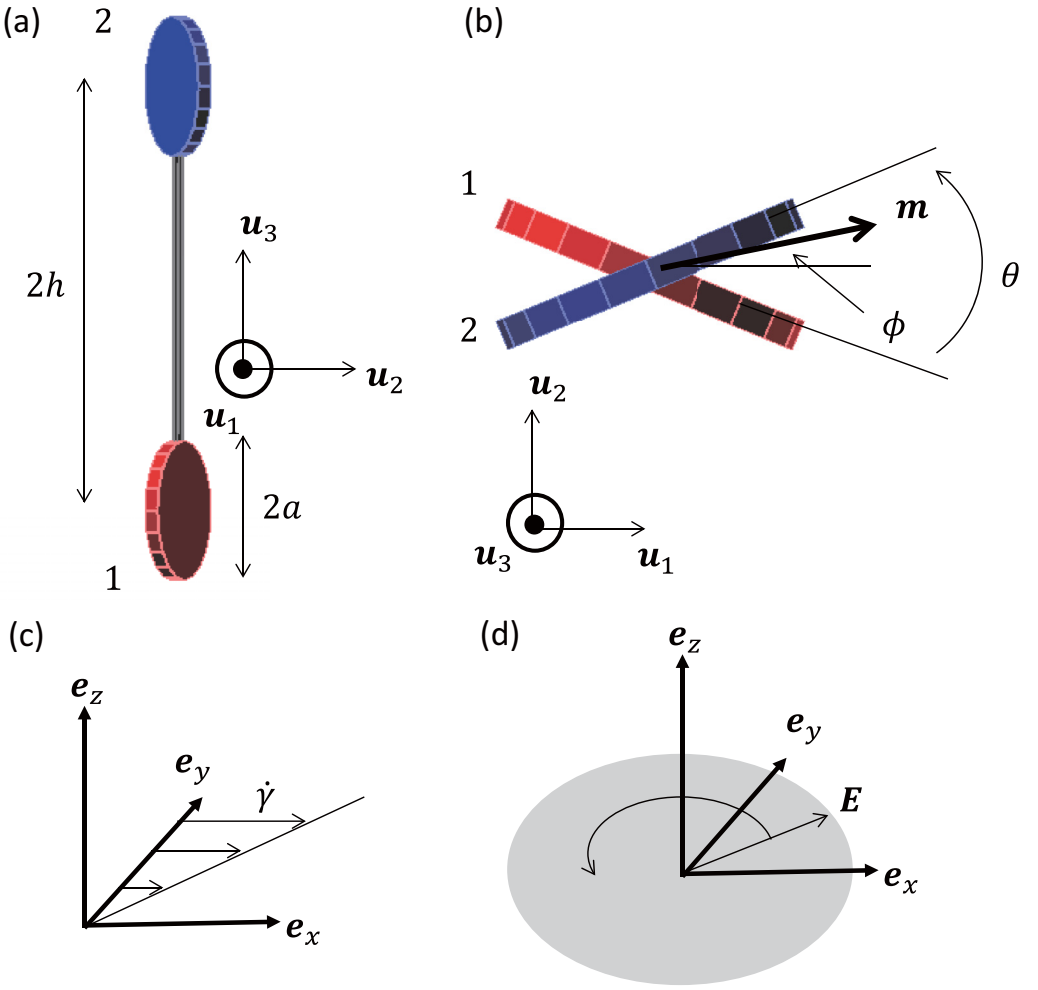

FIG. 1. (a) The propeller-like particle considered in this paper. Two disks of radius a are connected by a thin rod to give a disk-to-disk separation of $2h$. (b) The particle viewed from the $\boldsymbol{u}_3$ axis. θ is the angle between the two disks, and ϕ is the angle between $\boldsymbol{m}$ and $\boldsymbol{u}_1$. (c) The shear flow considered in this paper. (d) The rotating electric field considered in this paper.

We study this problem using a simple model particle, a propeller-like particle, as shown in Fig. 1. We consider two methods of separation, shear flow and rotating electric field, and calculate the migration velocity explicitly as a function of the particle structure and the field characteristic, such as the strength of the shear rate or electric field. Using these results, we discuss the chirality parameter, the parameter which specifies the degree of chirality.

This paper is organized as follows. A framework of the motion of a particle in an external field is presented in Sec. II. The mobility tensor of a propeller-like particle is calculated by superposition approximation and its spin-averaged tensor is shown in Sec. III. The conditions of the simulation method are written in Sec. IV. The migration in shear flow is discussed in Sec. V. The migration in a rotating electric field is discussed in Sec. VI. The relation between the structure of the particle and mobility is discussed in Sec. VII. Finally, we summarize our paper in Sec. VIII.

II. MOTION OF A PARTICLE IN AN EXTERNAL FIELD

A. Particle in external fields

The particle we consider in this paper in shown in Fig. 1. It consists of two thin disks of radius a rigidly fixed to a thin rod which we call the particle axis. The center-to-center distance between the disks is $2h$. The two disks make an angle θ with each other. The three parameters a, h, and θ completely specify the particle shape and its hydrodynamic properties.

To investigate the separation by electric fields, we assume that the particle has a permanent electric dipole $\boldsymbol{m}$ fixed to the particle parallel or perpendicular to the particle axis. If $\boldsymbol{m}$ is perpendicular to the axis, another structural parameter, ϕ, is needed, which is the angle that $\boldsymbol{m}$ makes against a plane bisecting the two disks [see Fig. 1(b)].

We take three orthogonal unit vectors $\boldsymbol{u}_1$, $\boldsymbol{u}_2$, and $\boldsymbol{u}_3$ fixed to the particle: $\boldsymbol{u}_3$ is along the particle axis, and $\boldsymbol{u}_1$ and $\boldsymbol{u}_2$ are the unit vectors in the plane bisecting the disk plane. If the dipole moment $\boldsymbol{m}$ is perpendicular to the particle axis, it is given by $\boldsymbol{m} = m(\cos\phi\boldsymbol{u}_1 + \sin\phi\boldsymbol{u}_2)$. If the dipole moment is parallel to the particle axis, $\boldsymbol{m}$ is given by $\boldsymbol{m} = m\boldsymbol{u}_3$.

We consider the motion of such a particle in a shear field and in an electric field. We let $\boldsymbol{e}_x$, $\boldsymbol{e}_y$, and $\boldsymbol{e}_z$ be the orthogonal unit vectors in the laboratory frame. We consider the shear flow in which the velocity at position $\boldsymbol{r}$ is given by [see Fig. 1(c)]

$$\boldsymbol{v}_0(\boldsymbol{r}) = \dot{\gamma}\boldsymbol{e}_x\boldsymbol{e}_y \cdot \boldsymbol{r}, \tag{1}$$

where $\dot{\gamma}$ is the shear rate. We also consider the electric field which is rotating around $\boldsymbol{e}_z$ with angular frequency ω [see Fig. 1(d)],

$$\boldsymbol{E}(t) = E(\cos\omega t\boldsymbol{e}_x + \sin\omega t\boldsymbol{e}_y). \tag{2}$$

Our objective here is to calculate the average of the particle velocity $\langle \boldsymbol{V} \rangle$ in such situations.

B. Brownian motion of particles of arbitrary shape

The dynamics of particles of arbitrary shape have been studied by many people [7–11]. Here we summarize the equations we use in our present calculations [12].

Consider a particle moving in a flow field, the velocity of which far from the particle is given by

$$\boldsymbol{v}_0(\boldsymbol{r}) = \boldsymbol{V}_0 + \boldsymbol{\Omega}_0 \times \boldsymbol{r} + \boldsymbol{E}_0 \cdot \boldsymbol{r}, \tag{3}$$

where $\boldsymbol{V}_0$, $\boldsymbol{\Omega}_0$, and $\boldsymbol{E}_0$ are constants representing the linear velocity, the angular velocity, and the strain rate tensor of the imposed flow, respectively. Suppose that the particle is moving with velocity $\boldsymbol{V}$ and angular velocity $\boldsymbol{\Omega}$ in such a velocity field. The hydrodynamic frictional force $\boldsymbol{F}_d$ and torque $\boldsymbol{T}_d$ exerted on the particle by the fluid are calculated by Stokesian hydrodynamics and can be written as

$$\begin{pmatrix} \boldsymbol{F}_d \\ \boldsymbol{T}_d \end{pmatrix} = -\begin{pmatrix} \boldsymbol{A} & \tilde{\boldsymbol{B}} \\ \boldsymbol{B} & \boldsymbol{C} \end{pmatrix} \cdot \begin{pmatrix} \boldsymbol{V} - \boldsymbol{V}_0 \\ \boldsymbol{\Omega} - \boldsymbol{\Omega}_0 \end{pmatrix} + \begin{pmatrix} \tilde{\boldsymbol{G}} \\ \tilde{\boldsymbol{H}} \end{pmatrix} : \boldsymbol{E}_0, \tag{4}$$

where $\boldsymbol{A}$, $\boldsymbol{B}$, $\tilde{\boldsymbol{B}}$, $\boldsymbol{C}$, $\tilde{\boldsymbol{G}}$, and $\tilde{\boldsymbol{H}}$ are tensors called the resistance tensors [7,8]. They are functions of the particle shape and particle orientation.

If the particle motion is induced by an external force $\boldsymbol{F}$ and an external torque $\boldsymbol{T}$, $\boldsymbol{V}$ and $\boldsymbol{\Omega}$ are determined by the force balance condition

$$\boldsymbol{F} + \boldsymbol{F}_d = 0, \quad \boldsymbol{T} + \boldsymbol{T}_d = 0. \tag{5}$$

The external force and the torque are derived from the external potential U:

$$\boldsymbol{F} = -\frac{\partial U}{\partial \boldsymbol{R}}, \quad \boldsymbol{T} = -\boldsymbol{R}U, \tag{6}$$

where $\boldsymbol{R}$ is the rotational differential operator defined by [6]

$$\boldsymbol{R} = \sum_i \boldsymbol{u}_i \times \frac{\partial}{\partial \boldsymbol{u}_i}. \tag{7}$$

Equations (4) and (5) give the following equation for the particle velocity:

$$\begin{pmatrix} \boldsymbol{V} \\ \boldsymbol{\Omega} \end{pmatrix} = \begin{pmatrix} \boldsymbol{V}_0 \\ \boldsymbol{\Omega}_0 \end{pmatrix} + \begin{pmatrix} \boldsymbol{a} & \tilde{\boldsymbol{b}} \\ \boldsymbol{b} & \boldsymbol{c} \end{pmatrix} \cdot \begin{pmatrix} \boldsymbol{F} \\ \boldsymbol{T} \end{pmatrix} + \begin{pmatrix} \tilde{\boldsymbol{g}} \\ \tilde{\boldsymbol{h}} \end{pmatrix} : \boldsymbol{E}_0, \tag{8}$$

where the mobility tensors $\boldsymbol{a}$, $\boldsymbol{b}$, $\tilde{\boldsymbol{b}}$, $\boldsymbol{c}$, $\tilde{\boldsymbol{g}}$, and $\tilde{\boldsymbol{h}}$ are given by

$$\begin{pmatrix} \boldsymbol{a} & \tilde{\boldsymbol{b}} \\ \boldsymbol{b} & \boldsymbol{c} \end{pmatrix} = \begin{pmatrix} \boldsymbol{A} & \tilde{\boldsymbol{B}} \\ \boldsymbol{B} & \boldsymbol{C} \end{pmatrix}^{-1} \tag{9}$$

and

$$\begin{pmatrix} \tilde{\boldsymbol{g}} \\ \tilde{\boldsymbol{h}} \end{pmatrix} = \begin{pmatrix} \boldsymbol{A} & \tilde{\boldsymbol{B}} \\ \boldsymbol{B} & \boldsymbol{C} \end{pmatrix}^{-1} \cdot \begin{pmatrix} \tilde{\boldsymbol{G}} \\ \tilde{\boldsymbol{H}} \end{pmatrix}. \tag{10}$$

If the particle is subject to Brownian motion, the equation is modified as

$$\begin{pmatrix} \boldsymbol{V} \\ \boldsymbol{\Omega} \end{pmatrix} = \begin{pmatrix} \boldsymbol{V}_0 \\ \boldsymbol{\Omega}_0 \end{pmatrix} + \begin{pmatrix} \boldsymbol{a} & \tilde{\boldsymbol{b}} \\ \boldsymbol{b} & \boldsymbol{c} \end{pmatrix} \cdot \begin{pmatrix} \boldsymbol{F} \\ \boldsymbol{T} \end{pmatrix} + \begin{pmatrix} \tilde{\boldsymbol{g}} \\ \tilde{\boldsymbol{h}} \end{pmatrix} : \boldsymbol{E}_0 + \begin{pmatrix} \boldsymbol{V}^B \\ \boldsymbol{\Omega}^B \end{pmatrix}, \tag{11}$$

where $\boldsymbol{V}^B$ and $\boldsymbol{\Omega}^B$ are stochastic vectors representing the thermal motion. Their averages are zero,

$$\langle \boldsymbol{V}^B(t) \rangle = 0, \quad \langle \boldsymbol{\Omega}^B(t) \rangle = 0, \tag{12}$$

and their time correlations are determined by the fluctuation dissipation relation:

$$\begin{aligned} \langle \boldsymbol{V}^B(t) \boldsymbol{V}^B(t') \rangle &= 2k_B T \boldsymbol{a} \delta(t - t'), \\ \langle \boldsymbol{\Omega}^B(t) \boldsymbol{\Omega}^B(t') \rangle &= 2k_B T \boldsymbol{c} \delta(t - t'), \\ \langle \boldsymbol{\Omega}^B(t) \boldsymbol{V}^B(t') \rangle &= 2k_B T \boldsymbol{b} \delta(t - t'). \end{aligned} \tag{13}$$

It should be noted that in rewriting the deterministic equation (8) to the Langevin equation (11), we have to add "divergence terms" such as $k_B T \boldsymbol{R} \cdot \tilde{\boldsymbol{b}}$ and $k_B T \boldsymbol{R} \cdot \boldsymbol{c}$ in order to ensure the equation is consistent with the Boltzmann distribution at equilibrium. However, such terms become zero in the present case. One can show for a general symmetric tensor $\boldsymbol{s}$ which is a function of $\boldsymbol{u}_1$, $\boldsymbol{u}_2$, and $\boldsymbol{u}_3$ that $\boldsymbol{R} \cdot \boldsymbol{s}$ is zero. The tensor $\boldsymbol{c}$ is symmetric from the reciprocal relation, and the tensor $\boldsymbol{b}$ can be made symmetric if we choose the center of mobility [8] at the center of the particle.

The mobility tensors $\boldsymbol{a}$, $\boldsymbol{b}$, etc. depend on the orientation of the particle and vary with time. It is convenient to express them using the particle frame since their components in the particle frame are constant, independent of time. For example, the tensors $\boldsymbol{b}$ and $\boldsymbol{c}$ are written as

$$\boldsymbol{b}(t) = \sum_{ij=1,2,3} b_{ij} \boldsymbol{u}_i(t) \boldsymbol{u}_j(t), \quad \boldsymbol{c}(t) = \sum_{ij=1,2,3} c_{ij} \boldsymbol{u}_i(t) \boldsymbol{u}_j(t), \tag{14}$$

where b_{ij} and c_{ij} are constants which depend on the shape of the particle but are independent of time.

In the following calculation, we take $\boldsymbol{u}_1$, $\boldsymbol{u}_2$, and $\boldsymbol{u}_3$ along the principal axes of the tensor $\boldsymbol{c}$. Then

$$c_{ij} = c_i \delta_{ij}, \tag{15}$$

where c_i $(i = 1,2,3)$ are the principal values of the tensor $\boldsymbol{c}$.

If the particle is moving in a shear flow described by Eq. (1) without any external forces, the migration velocity is given by

$$\boldsymbol{V} = \tilde{\boldsymbol{g}} : \boldsymbol{E}_0 + \boldsymbol{V}^B, \tag{16}$$

where $\boldsymbol{E}_0 = \dot{\gamma}(\boldsymbol{e}_x \boldsymbol{e}_y + \boldsymbol{e}_y \boldsymbol{e}_x)/2$.

If the particle is moving in a rotating electric field described by Eq. (2), the migration velocity is given by

$$\boldsymbol{V} = \boldsymbol{b} \cdot \boldsymbol{T} + \boldsymbol{V}^B, \tag{17}$$

where the torque $\boldsymbol{T}$ is given by $\boldsymbol{T} = \boldsymbol{m} \times \boldsymbol{E}$.

In both situations, we calculate the average of the z component of the migration velocity:

$$\langle V_z \rangle = \langle (\tilde{\boldsymbol{g}} : \boldsymbol{E}_0)_z \rangle, \quad \langle V_z \rangle = \langle (\boldsymbol{b} \cdot \boldsymbol{T})_z \rangle. \tag{18}$$

III. MOBILITY TENSOR OF PROPELLER-LIKE PARTICLES

We now calculate the mobility tensor of the propeller-like particle shown in Fig. 1(a). We use the superposition approximation [8] that the resistance tensor of the propeller-like particle is a sum of the contribution of two disks. The resistance tensors of a disk of radius a are given by

$$\begin{aligned} &A_{ij}^{(0)} = \frac{16}{3}\eta a(n_i n_j + 2\delta_{ij}), \quad B_{ij}^{(0)} = 0, \quad C_{ij}^{(0)} = \frac{32}{3}\eta a^3 \delta_{ij}, \\ &\tilde{G}_{ijk}^{(0)} = 0, \quad \tilde{H}_{ijk}^{(0)} = -\frac{16}{3}\eta a^3 (e_{ikl} n_l n_j + e_{jkl} n_i n_l), \end{aligned} \tag{19}$$

where η, e_{ikl}, and $\boldsymbol{n}$ are the fluid viscosity, the Levi-Civita symbol, and the unit vector normal to the disk, respectively.

When the propeller-like particle moves with translational velocity $\boldsymbol{V}$ and rotates at angular velocity $\boldsymbol{\Omega}$ around the center of the particle (i.e., the midpoint of the connecting rod), disks 1 and 2 of the propeller move with velocity $\boldsymbol{V} - h\boldsymbol{\Omega} \times \boldsymbol{u}_3$ and $\boldsymbol{V} + h\boldsymbol{\Omega} \times \boldsymbol{u}_3$, respectively, and rotate with angular velocity $\boldsymbol{\Omega}$. The resistance tensors of the propeller-like particle are obtained by the summation of each contribution:

$$\boldsymbol{A} = \boldsymbol{A}^{(1)} + \boldsymbol{A}^{(2)}, \quad \boldsymbol{B} = \boldsymbol{B}^{(1)} + \boldsymbol{B}^{(2)}, \ldots. \tag{20}$$

The explicit form of the resistance tensors $\boldsymbol{A}^{(p)}$ and $\boldsymbol{B}^{(p)}$ ($p = 1,2$) are given as

$$A_{ij}^{(p)} = \frac{16}{3}\eta a\left(n_i^{(p)} n_j^{(p)} + 2\delta_{ij}\right), \quad B_{ij}^{(p)} = (-1)^p \frac{16}{3}\eta a h e_{ikl} u_{3k}\left(n_l^{(p)} n_j^{(p)} + 2\delta_{lj}\right), \tag{21}$$

where $\boldsymbol{n}^{(p)}$ is the unit vector normal to the disk p. Using the twist angle θ between the disks, $\boldsymbol{n}^{(1)}$ and $\boldsymbol{n}^{(2)}$ are written as

$$\boldsymbol{n}^{(1)} = \sin(\theta/2)\boldsymbol{u}_1 + \cos(\theta/2)\boldsymbol{u}_2, \quad \boldsymbol{n}^{(2)} = -\sin(\theta/2)\boldsymbol{u}_1 + \cos(\theta/2)\boldsymbol{u}_2. \tag{22}$$

Other resistance tensors are calculated in the same way and are given by

$$\begin{aligned} C_{ij}^{(p)} &= \frac{16}{3}\eta a\left\{2a^2\delta_{ij} + h^2 e_{ikl} e_{jmn} u_{3k} u_{3n}\left(n_l^{(p)} n_m^{(p)} + 2\delta_{lm}\right)\right\}, \\ \tilde{G}_{ijk}^{(p)} &= (-1)^p \frac{8}{3}\eta a h\left\{u_{3k}\left(n_j^{(p)} n_i^{(p)} + 2\delta_{ji}\right) + u_{3j}\left(n_k^{(p)} n_i^{(p)} + 2\delta_{ik}\right)\right\}, \\ \tilde{H}_{ijk}^{(p)} &= \frac{16}{3}\eta a^3\left(e_{ikl} n_j^{(p)} n_l^{(p)} + e_{ijl} n_k^{(p)} n_l^{(p)}\right) \\ &\quad + \frac{8}{3}\eta a h^2\{(\sin^2(\theta/2)+2)(u_{2i}u_{3j}u_{1k} + u_{2i}u_{1j}u_{3k}) - (\cos^2(\theta/2)+2)(u_{1i}u_{3j}u_{2k} + u_{1i}u_{2j}u_{3k}) \\ &\quad - (-1)^p \sin(\theta/2)\cos(\theta/2)(u_{2i}u_{3j}u_{2k} - u_{1i}u_{3j}u_{1k} + u_{2i}u_{2j}u_{3k} - u_{1i}u_{1j}u_{3k})\}. \end{aligned} \tag{23}$$

The mobility tensors are then obtained by Eq. (10). The final results of that calculation are as follows:

$$\boldsymbol{a} = \frac{3}{64\eta a}\left\{\frac{2a^2 + h^2(\cos^2(\theta/2)+2)}{3h^2 + a^2(\sin^2(\theta/2)+2)}\boldsymbol{u}_1\boldsymbol{u}_1 + \frac{2a^2 + h^2(\sin^2(\theta/2)+2)}{3h^2 + a^2(\cos^2(\theta/2)+2)}\boldsymbol{u}_2\boldsymbol{u}_2 + \boldsymbol{u}_3\boldsymbol{u}_3\right\}, \quad (24)$$

$$\boldsymbol{b} = \frac{3}{64\eta a}\left\{-\frac{1}{2}\frac{h\sin\theta}{3h^2 + a^2(\sin^2(\theta/2)+2)}\boldsymbol{u}_1\boldsymbol{u}_1 + \frac{1}{2}\frac{h\sin\theta}{3h^2 + a^2(\cos^2(\theta/2)+2)}\boldsymbol{u}_2\boldsymbol{u}_2\right\}, \quad (25)$$

$$\boldsymbol{c} = \frac{3}{64\eta a}\left\{\frac{2+\sin^2(\theta/2)}{3h^2 + a^2(\sin^2(\theta/2)+2)}\boldsymbol{u}_1\boldsymbol{u}_1 + \frac{2+\cos^2(\theta/2)}{3h^2 + a^2(\cos^2(\theta/2)+2)}\boldsymbol{u}_2\boldsymbol{u}_2 + \frac{1}{a^2}\boldsymbol{u}_3\boldsymbol{u}_3\right\}, \quad (26)$$

$$\tilde{\boldsymbol{g}} = -\frac{a^2 h\sin\theta}{4}\left\{\frac{\sin^2(\theta/2)}{3h^2 + a^2(\sin^2(\theta/2)+2)}(\boldsymbol{u}_1\boldsymbol{u}_2\boldsymbol{u}_3 + \boldsymbol{u}_1\boldsymbol{u}_3\boldsymbol{u}_2) + \frac{\cos^2(\theta/2)}{3h^2 + a^2(\cos^2(\theta/2)+2)}(\boldsymbol{u}_2\boldsymbol{u}_1\boldsymbol{u}_3 + \boldsymbol{u}_2\boldsymbol{u}_3\boldsymbol{u}_1)\right\}, \quad (27)$$

$$\tilde{\boldsymbol{h}} = -\frac{1}{2}\frac{3h^2 + a^2\cos^2(\theta/2)(\sin^2(\theta/2)+2)}{3h^2 + a^2(\sin^2(\theta/2)+2)}(\boldsymbol{u}_1\boldsymbol{u}_2\boldsymbol{u}_3 + \boldsymbol{u}_1\boldsymbol{u}_3\boldsymbol{u}_2) + \frac{1}{2}\frac{3h^2 + a^2\sin^2(\theta/2)(\cos^2(\theta/2)+2)}{3h^2 + a^2(\cos^2(\theta/2)+2)}(\boldsymbol{u}_2\boldsymbol{u}_1\boldsymbol{u}_3 + \boldsymbol{u}_2\boldsymbol{u}_3\boldsymbol{u}_1) + \frac{1}{2}\cos\theta(\boldsymbol{u}_3\boldsymbol{u}_1\boldsymbol{u}_2 + \boldsymbol{u}_3\boldsymbol{u}_2\boldsymbol{u}_1). \quad (28)$$

Spin-averaged mobility tensor

Analysis of the rotational Brownian motion of a rigid particle of arbitrary shape becomes complex since one has to deal with the motion of three orthogonal vectors $\boldsymbol{u}_1$, $\boldsymbol{u}_2$, and $\boldsymbol{u}_3$. For particles with large aspect ratios, spin-averaged approximation has been introduced to simplify such calculations [3]. The approximation is used in migration of the particle in weak shear flow shown in Sec. V. In this approximation, the mobility tensor, $\boldsymbol{a}$, is replaced by the average $\langle\boldsymbol{a}\rangle_{\text{spin}}$ where the average $\langle\cdots\rangle_{\text{spin}}$ stands for the average over the rotation around $\boldsymbol{u}_3$. Furthermore, in calculating the average $\langle\cdots\rangle_{\text{spin}}$, it is assumed that the distribution of $\boldsymbol{u}_1$ and $\boldsymbol{u}_2$ are completely random around $\boldsymbol{u}_3$. With such an assumption, it is easy to show

$$\langle\boldsymbol{u}_1\boldsymbol{u}_1\rangle_{\text{spin}} = \langle\boldsymbol{u}_2\boldsymbol{u}_2\rangle_{\text{spin}} = \tfrac{1}{2}(\boldsymbol{I} - \boldsymbol{u}_3\boldsymbol{u}_3). \quad (29)$$

This gives, for example,

$$\langle\boldsymbol{a}\rangle_{\text{spin}} = \frac{3}{64\eta a}\left\{\frac{1}{3}(\cos^2(\theta/2)+2)\langle\boldsymbol{u}_1\boldsymbol{u}_1\rangle_{\text{spin}} + \frac{1}{3}(\sin^2(\theta/2)+2)\langle\boldsymbol{u}_2\boldsymbol{u}_2\rangle_{\text{spin}} + \boldsymbol{u}_3\boldsymbol{u}_3\right\} = \frac{3}{64\eta a}\frac{1}{6}(5\boldsymbol{I} + \boldsymbol{u}_3\boldsymbol{u}_3), \quad (30)$$

where terms of higher order in (a/h) are ignored. Similar calculations can be done for other tensors. The detailed calculations are given in the Appendix, and the final results are

$$\langle\boldsymbol{a}\rangle_{\text{spin}} = \frac{3}{64\eta a}\frac{1}{6}(5\boldsymbol{I} + \boldsymbol{u}_3\boldsymbol{u}_3), \quad (31)$$

$$\langle\boldsymbol{b}\rangle_{\text{spin}} = -\frac{1}{1536\eta h a}\sin 2\theta\left(\frac{a}{h}\right)^2(\boldsymbol{I} - \boldsymbol{u}_3\boldsymbol{u}_3), \quad (32)$$

$$\langle \boldsymbol{c} \rangle_{\rm spin} = \frac{3}{64\eta a}\left[\frac{5}{6h^2}(\boldsymbol{I} - \boldsymbol{u}_3\boldsymbol{u}_3) + \frac{1}{a^2}\boldsymbol{u}_3\boldsymbol{u}_3\right], \tag{33}$$

$$\langle \tilde{g} \rangle_{{\rm spin},ijk} = -\frac{a^2 \sin 2\theta}{48h}(e_{ilj}u_{3l}u_{3k} + e_{ilk}u_{3l}u_{3j}), \tag{34}$$

and

$$\langle \tilde{h} \rangle_{{\rm spin},ijk} = e_{ilj}u_{3l}u_{3k} + e_{ilk}u_{3l}u_{3j}. \tag{35}$$

IV. SIMULATION METHOD

To simulate the Brownian motion of the particle, we first calculated the mobility tensor components in the particle frame. The matrix in Eq. (9) is Cholesky decomposed only once to include the Brownian displacement [13]. We then conducted a simulation of the rotational Brownian motion using Eqs. (11) and (14). We used quaternions to describe the rotation [14]. In our simulation, we included the random angular velocity $\boldsymbol{\Omega}^B$ but did not include the random velocity $\boldsymbol{V}^B$, since $\boldsymbol{V}^B$ does not affect the average value $\langle V_z \rangle$, and inclusion of the term only increases the statistical error.

The set of differential equations is numerically solved by the fourth-order Runge-Kutta method. The time difference between time steps is $dt = 0.001/\dot{\gamma}$ in the shear flow or $dt = 0.001/\omega$ in the rotating electric field.

We conducted Brownian motion simulations for particles whose length $h/a = 3$. The particles were initially in random orientations, and we calculated the average migration velocity $\langle V_z \rangle$ with 1000 particles. Our results are independent of the initial orientation when the simulation time and number of the particles are appropriately large. The results are discussed in subsequent sections, where the standard errors in each data set are about the same size of each symbol.

V. MIGRATION OF PROPELLER-LIKE PARTICLES IN SHEAR FLOW

A. Results of simulation

Figures 2 and 3 show how the migration velocity $\langle V_z \rangle$ of a propeller-like particle in a shear flow changes with the shear rate $\dot{\gamma}$. In Fig. 2, $\langle V_z \rangle / a\dot{\gamma}$ is plotted against the Péclet number ${\rm Pe} = \dot{\gamma}/D_r$, where D_r is the rotational diffusion constant associated with the rotation of the particle axis. D_r is given by $D_r = k_B T(c_1 + c_2)/2$, where c_1 and c_2 are the first two smallest eigenvalues of the tensor $\boldsymbol{c}$.

As seen in Fig. 2, the average migration velocity $\langle V_z \rangle$ is zero if θ is equal to zero or $\pm\pi/2$. This is natural, since the particle is not chiral for these angles. If θ is different from these values, $\langle V_z \rangle$ becomes

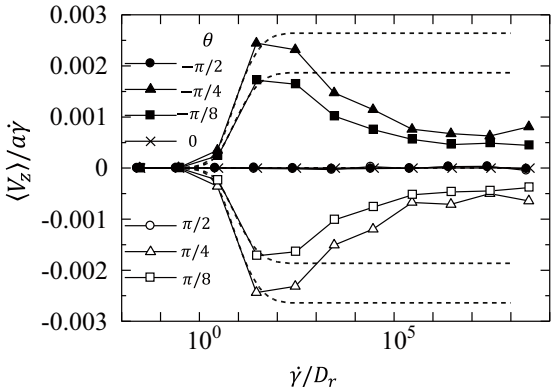

FIG. 2. Migration velocity $\langle V_z \rangle / a\dot{\gamma}$ of a propeller particle in simple shear flow plotted as a function of the Péclet number $\dot{\gamma}/D_r$. Symbols show the results of simulation. The dashed lines show Eq. (36).

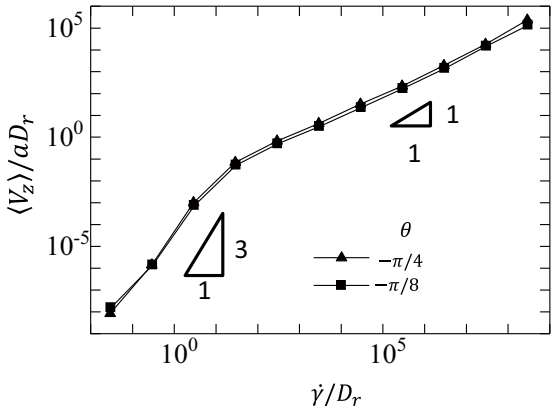

FIG. 3. Migration velocity $\langle V_z\rangle/aD_r$ (normalized by aD_r) of a propeller particle in simple shear flow plotted as a function of the Péclet number $\dot{\gamma}/D_r$.

nonzero. It is seen that the migration velocity of particles having $-\theta$ is the opposite of that of particles having θ. These results are consistent with the mirror symmetry of the equation of motion in fluids.

We now discuss in more detail how the migration velocity $\langle V_z\rangle$ depends on the shear rate $\dot{\gamma}$, and the twist angle θ.

B. Shear rate dependence

Figure 3 shows $\langle V_z\rangle/aD_r$ against Péclet number $\dot{\gamma}/D_r$ in a double logarithmic plot. It is seen that $\langle V_z\rangle$ increases with an increase in $\dot{\gamma}$, and that the slope decreases with an increase in $\dot{\gamma}$. This result can be understood as follows.

For small Péclet numbers, it has been predicted that $\langle V_z\rangle$ increases with the power law $\langle V_z\rangle \propto \dot{\gamma}^3$. This is because (a) the migration velocity $\langle V_z\rangle$ must be an odd function of $\dot{\gamma}$, and (b) the linear term is zero since the linear coupling between the vectorial quantity $\langle \boldsymbol{V}\rangle$ and the tensorial quantity $\boldsymbol{E}_0$ is not allowed (Curie's law) [2,3]. This prediction is consistent with Fig. 3, where the slope of 3 is shown by the first triangle.

On the other hand, for large Péclet numbers, it is seen that $\langle V_z\rangle$ increases linearly with $\dot{\gamma}$. (This is also seen in Fig. 2, where the plot $\langle V_z\rangle/a\dot{\gamma}$ approaches a constant value for large Péclet numbers). This is reasonable since for large Péclet numbers, Brownian motion is negligible and dimensional analysis indicates that $\langle V_z\rangle$ must be proportional to $\dot{\gamma}$.

Theoretical calculations can be done for $\langle V_z\rangle$ if we use the spin-averaged mobility tensor. By use of Eqs. (A6), (A7), and (18), the migration velocity $\langle V_z\rangle$ is written as

$$\langle V_z\rangle = (\langle\tilde{\boldsymbol{g}}\rangle_{\rm spin} : \boldsymbol{E}_0)_z = \frac{\dot{\gamma}\, g_{\rm spin}}{2}\langle u_{3x}^2 - u_{3y}^2\rangle, \tag{36}$$

where $g_{\rm spin} = a^2 \sin 2\theta/(24h)$. For small Péclet numbers, the average $\langle u_{3x}^2 - u_{3y}^2\rangle$ is proportional to $(\dot{\gamma}/D_r)^2$. For large Péclet numbers $\langle u_{3x}^2 - u_{3y}^2\rangle$ approaches a finite constant value. This gives the shear rate dependence discussed above. The dashed line in Fig. 2 is calculated by using the results for $\langle u_{3x}^2 - u_{3y}^2\rangle$ for a uniaxial particle [15]. Good agreement is seen between such calculations and the simulation if $\dot{\gamma}/D_r$ is less than $\approx$10.

Deviation between the calculated values and the simulation is seen for larger Péclet numbers. Examination of the results indicates that it is because the spin-averaged approximation becomes inaccurate at large Péclet numbers. Figure 4 shows the orientational order parameters. The spin-averaged approximation assumes $\langle \boldsymbol{u}_1\boldsymbol{u}_1\rangle = \langle \boldsymbol{u}_2\boldsymbol{u}_2\rangle$, but such equality does not hold for large Péclet number, as seen in Fig. 4.

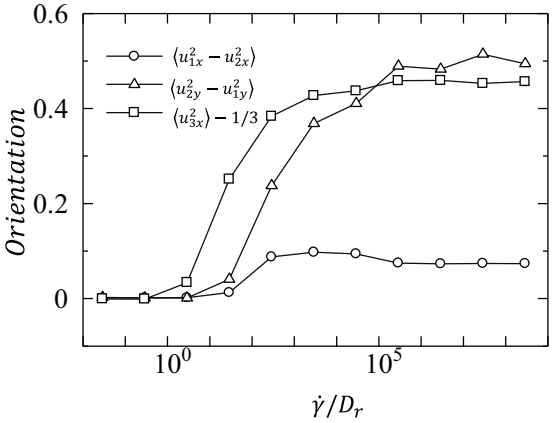

FIG. 4. Orientations $\langle u_{1x}^2 - u_{2x}^2 \rangle$, $\langle u_{2y}^2 - u_{1y}^2 \rangle$, and $\langle u_{3x}^2 \rangle - 1/3$ of a propeller-like particle with $\theta = \pi/4$ are shown as a function of the Péclet number $\dot{\gamma}/D_r$ in simple shear flow.

Despite the failure in the quantitative prediction at large Péclet numbers, the spin-averaged approximation predicts correctly the overall behavior of the shear-rate dependence of the migration velocity. This is also seen in the structural dependence of the migration velocity which is discussed in the next section.

C. Structure dependence

We now discuss how the migration velocity depends on the structure of the particle. Figure 5 shows the plot of $\langle V_z \rangle / a\dot{\gamma}$ against the twist angle θ at various Péclet numbers. It is seen that the simulation result is well fitted by the curve const $\times \sin 2\theta$ for all Péclet numbers.

The functional form of $\sin 2\theta$ is what one might expect. The migration velocity must vanish when θ is equal to zero and $\pi/2$ (as was discussed in Sec. III), and $\sin 2\theta$ is the simplest periodic function satisfying this condition. The $\sin 2\theta$ dependence can be derived theoretically if the spin-averaged approximation [Eq. (33)] is used.

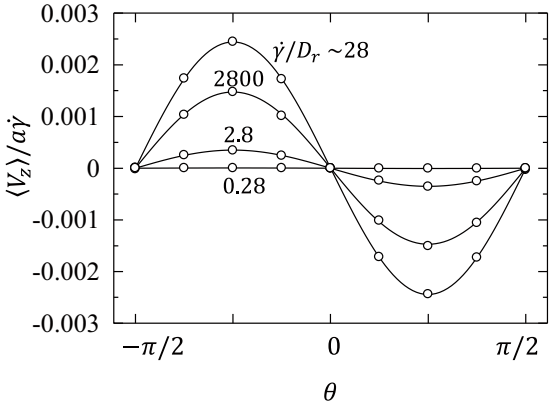

FIG. 5. Migration velocity $\langle V_z \rangle / a\dot{\gamma}$ of a propeller particle in simple shear flow plotted as a function of the angle θ. Symbols show the results of simulation. Lines show the curve $\langle V_z \rangle / a\dot{\gamma} = \alpha \sin 2\theta$, where α is a fitting parameter.

To summarize, the migration velocity of a propeller in shear flow is given by the following equation:

$$\langle V_z \rangle \sim \begin{cases} \frac{1}{a^2}\frac{(a\dot{\gamma})^3}{D_r^2}\sin 2\theta & \text{for} \frac{\dot{\gamma}}{D_r} \ll 1, \\ a\dot{\gamma}\sin 2\theta & \text{for} \frac{\dot{\gamma}}{D_r} \gg 1. \end{cases} \tag{37}$$

VI. MIGRATION OF PROPELLER-LIKE PARTICLES IN A ROTATING ELECTRIC FIELD

A. Mobility of propeller-like particles in weak electric fields

Using the same method as in the previous section, we have conducted simulations for propeller-like particles having a permanent dipole moment placed in a rotating electric field. Before presenting the results, we first show the theoretical results which are valid for weak electric fields.

In weak electric fields, the time-averaged migration velocity is proportional to E^2 and can be written as [6]

$$\langle V_z \rangle = M(\omega)E^2, \tag{38}$$

where the coefficient $M(\omega)$ is expressed by the mobility tensor $\boldsymbol{b}$ representing the translation-rotation coupling,

$$M(\omega) = \sum_{i,j=1}^{3} \left(b_{ii}m_j^2 - b_{ij}m_i m_j\right)\frac{1}{6k_BT}\frac{\omega\tau_j}{1+(\omega\tau_j)^2}, \tag{39}$$

and τ_i $(i = 1,2,3)$ is the dielectric relaxation time given by

$$\tau_i = \frac{1}{k_BT\left(\sum_j c_j - c_i\right)}. \tag{40}$$

For the present propeller-like particle, the tensors b_{ij} and c_i are calculated by Eqs. (25) and (26), and Eqs. (39) and (40) give the following expression for the mobility $M(\omega)$ (here we only give an expression in the limit of $h \gg a$):

(a) In the case that the dipole is perpendicular to the main axis, i.e., $\boldsymbol{m} = m(\cos\phi\boldsymbol{u}_1 + \sin\phi\boldsymbol{u}_2)$,

$$M(\omega) = \frac{1}{6ah\eta k_BT}\frac{m^2\sin\theta\cos 2\phi}{128}\frac{\omega\tau}{1+(\omega\tau)^2}, \tag{41}$$

where

$$\tau = \frac{64\eta a^3}{3k_BT}. \tag{42}$$

(b) In the case that the dipole is parallel to the main axis, i.e., $\boldsymbol{m} = m\boldsymbol{u}_3$,

$$M(\omega) = -\frac{1}{6ah\eta k_BT}\frac{m^2\sin 2\theta}{768}\left(\frac{a}{h}\right)^2\frac{\omega\tau}{1+(\omega\tau)^2}, \tag{43}$$

where

$$\tau = \frac{64\eta a h^2}{5k_BT}. \tag{44}$$

In the following section, we discuss the results of the simulations in comparison with these results. The results for weak electric fields are not shown here since such a comparison was reported in our previous paper [6]. Here we mainly focus on the results of strong electric fields.

B. Dipole moment perpendicular to axis of the propeller-like particle

Figure 6 shows the migration velocity of a particle which has a dipole moment parallel to $\boldsymbol{u}_1$, plotted against the field strength E (normalized by k_BT/m) for various twist angles θ. The frequency

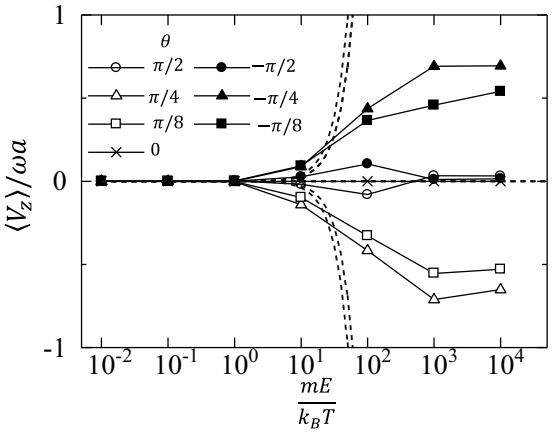

FIG. 6. Migration velocity $\langle V_z\rangle/\omega a$ of a propeller-like particle having dipole moment perpendicular to the axis, placed in rotating electric field, plotted as a function of mE/k_BT. Symbols show the results of simulation.

ω was chosen as $1/\tau$. The effect of the frequency was discussed in the previous paper [6], according to which the migration velocity becomes largest at the frequency $\omega = 1/\tau$.

It is seen that the curves in Fig. 6 have mirror symmetry with respect to the horizontal axis: the migration velocity of a particle having angle $-\theta$ is the opposite of that of a particle having angle θ.

The dashed lines in Fig. 6 indicate the theoretical curves obtained for weak fields. For weak fields, the migration velocity increases with the increase of field strength in proportion to E^2, which is consistent with our simulation. The result of the simulation deviates significantly from the dashed line for a strong electric field. This is because the orientation of the dipole moment is saturated in a strong electric field. In the strong-field limit, the migration velocity is determined by the angular frequency of the field and is independent of the field strength. This is seen in the result of the simulation (Fig. 6).

Figures 7 and 8 show how the migration velocity depends on the structure of the particle. Figure 7 shows the dependence on the twist angle θ. Unlike the shear flow, the migration velocity does not vanish at $\theta = \pm\pi/2$. This is because, due to the presence of the dipole moment, the particle remains chiral even at the angle $\theta = \pm\pi/2$. The solid lines in Fig. 7 denote the curves of $\sin\theta$.

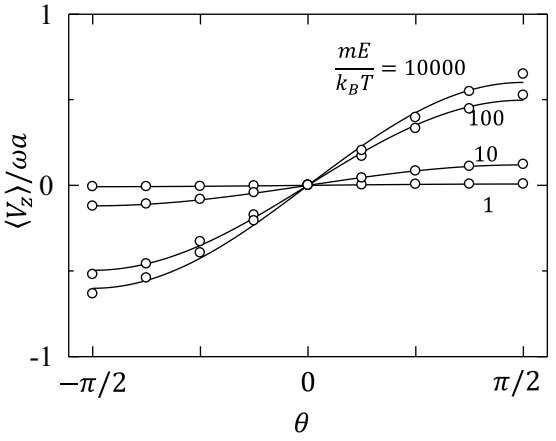

FIG. 7. Migration velocity $\langle V_z\rangle/a\omega$ of a propeller-like particle having dipole moment perpendicular to the axis plotted as a function of the angle θ. Symbols show the results of simulation. Lines show the curve $\langle V_z\rangle/\omega a = \alpha\sin\theta$, where α is a fitting parameter.

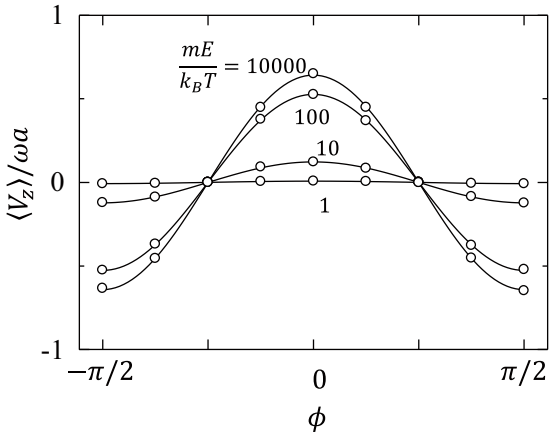

FIG. 8. Migration velocity $\langle V_z \rangle / \omega a$ of a propeller-like particle having dipole moment perpendicular to the axis plotted as a function of the angle ϕ. Symbols show the results of simulation. Lines show the curve $\langle V_z \rangle / \omega a = \alpha \cos 2\phi$, where α is a fitting parameter.

If the field is weak, the migration velocity should be calculated analytically. Equation (41) indicates that the migration velocity depends on θ and ϕ as $\langle V_z \rangle \propto \sin\theta \cos 2\phi$. Figure 7 indicates this angle dependence holds even for a strong field. The same is true for the ϕ dependence. Figure 8 indicates that the weak-field result $\langle V_z \rangle \propto \cos 2\phi$ holds even for a strong field. This is because ϕ is related to the particle structure.

C. Dipole moment parallel to axis of the propeller-like particle

Figure 9 shows the migration velocity of a particle which has a dipole moment parallel to the particle axis. Unlike the particle having a perpendicular dipole moment, this particle becomes nonchiral when $\theta = \pm\pi/2$. Therefore, the migration velocity vanishes at these angles.

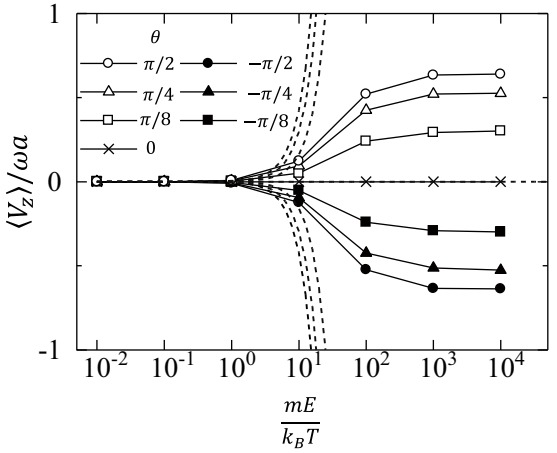

FIG. 9. Migration velocity $\langle V_z \rangle / a\omega$ of a propeller-like particle having dipole moment parallel to the axis plotted as a function of mE/k_BT. Symbols show the results of simulation.

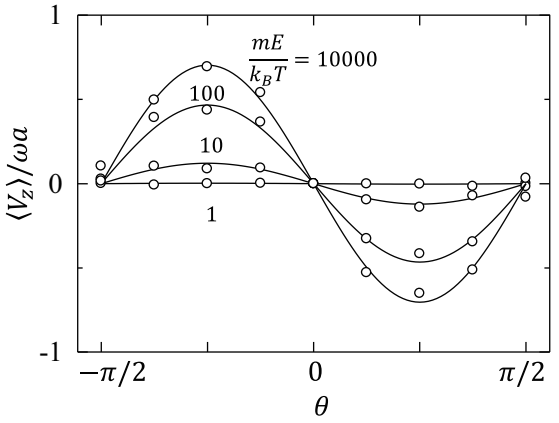

FIG. 10. Migration velocity $\langle V_z\rangle/a\omega$ of a propeller-like particle having dipole moment parallel to the axis plotted as a function of the angle θ in a rotating electric field. Symbols show the results of simulation. Lines show the curves $\langle V_z\rangle/\omega a = \alpha \sin 2\theta$, where α is a fitting parameter.

Figure 10 shows the twist angle dependence of the migration velocity $\langle V_z\rangle$. It is seen that $\langle V_z\rangle$ depends on the twist angle θ in the same way as in the shear flow, $\langle V_z\rangle \propto \sin 2\theta$. This angle dependence is the same as that predicted by the theory for a weak field [Eq. (43)].

VII. DISCUSSION

For a propeller-like particle, the particle is not chiral for $\theta = 0$, and the migration velocity is zero in cases of both shear and electric fields. The migration velocity becomes nonzero as θ deviates from zero, but the θ dependence is different for different types of fields and different types of particles.

In the shear flow, the migration velocity is proportional to $\sin 2\theta$. In the rotating electric field, on the other hand, the migration velocity is proportional to $\sin\theta \cos 2\phi$ if the dipole is perpendicular to the particle axis, and is proportional to $\sin 2\theta$ if the dipole is parallel to the particle axis. The reason for this is shown graphically in Fig. 11.

If the particle does not have a dipole moment (or if the dipole moment is parallel to the axis), the two particles a-1 and a-3 in Fig. 11 are identical, and the particles a-2 and a-4 are also identical. Therefore, the migration velocity of a particle with twist angle θ is equal to that with twist angle $\theta + \pi$; i.e., the migration velocity has a periodicity π as a function of θ. On the other hand, if the particle has a dipole moment perpendicular to the axis (with $\phi = 0$), the four particles b-1, b-2, b-3, and b-4 are all different, and the periodicity of the migration velocity is now 2π.

Whether a particle is chiral or not depends not only on the geometrical structure of the particle but also on other physical characteristics (such as the dipole moment) of the particle. This means that "chirality" depends on the experimental method by which we distinguish particles. For example, the propeller-like particle having twist angle $\pi/2$ is not regarded as chiral from the structural viewpoint. Indeed they cannot be separated by hydrodynamic methods which act on the geometrical shape only. On the other hand, if such particles have dipole moments perpendicular to the particle axis, they become chiral and the particles and their mirror-image particles behave differently in a rotating electric field. As was discussed by Harris *et al.* [1], there is no unique way of defining the chiral parameters. A practical way of defining the chiral parameters is to use the migration velocity associated with a certain separation method.

Finally, we provide an estimate of the migration velocity. We consider a propeller particle of size $a = h/3 \sim 1$ nm. In a shear flow of shear rate $\dot{\gamma} \sim 10^3$ 1/s, where the radius of a concentric cylinder is 10 cm and gap distance 1 mm and rotating speed 100 rpm are assumed, the migration velocity is estimated to be $\langle V_z\rangle \sim 10^{-25}$ m/s (viscosity $\eta \sim 1$ mPa s temperature $k_BT \sim 4.12 \times 10^{-21}$ J), which

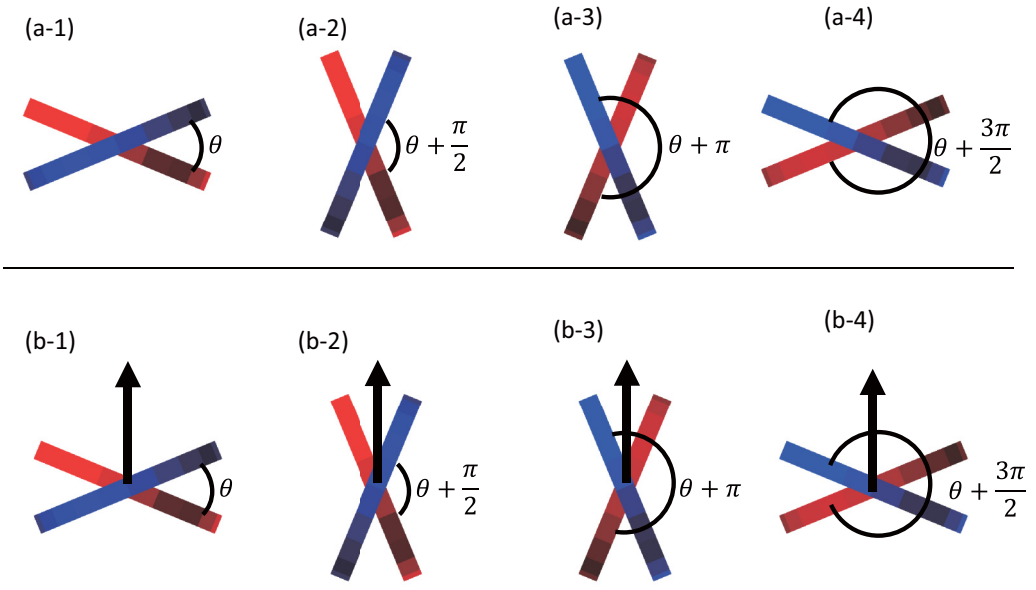

FIG. 11. Top views of the propeller-like particles for various twist angles. The reds and blues show disks 1 and 2, respectively. The black arrows show the dipole moments. Particles a-1 through a-4 are without dipole moment. Particles a-1 and a-3, and a-2 and a-4, are completely identical particles. Particles b-1 through b-4 are with dipole moment. All particles from b-1 to b-4 are different.

is too small for separation. On the other hand, using similar parameters as in Ref. [4], under a rotating electric field of strength $E \sim 10^6$ V/m and angular frequency $\omega \sim 10^8$ 1/s, $\langle V_z \rangle \sim 10^{-8}$ m/s for the perpendicular dipole moment and $\langle V_z \rangle \sim 10^{-10}$ m/s for the parallel dipole moment (the magnitude of the dipole moment is assumed to be $m \sim 10^{-29}$ C m). Therefore, separation by rotating electric field is feasible. If the particle is large, the separation becomes possible by shear flow: if $a \sim 1$ μm, the separation speed is $\langle V_z \rangle \sim 10^{-8}$ m/s, $\sim 10^{-3}$ m/day.

VIII. SUMMARY

We theoretically studied two methods of separating one type of propeller-like particles from their mirror-image particles. We calculated the migration velocity in a shear flow and in a rotating electric field, and showed how they depend on the field strength and also on particle structure. We explicitly demonstrated that a hydrodynamically nonchiral particle can be chiral if it has a dipole moment. We also demonstrated that the spin-averaged approximation works well: the characteristic aspects of such structure dependence are in accordance with the results obtained using this approximation.

ACKNOWLEDGMENTS

This work is supported in part by NSFC (Grants No. 21434001 and No. 11421110001), Ministry of Education, Culture, Sports, Science and Technology (MEXT), Japan Science and Technology Agency (JST), and JSPS KAKENHI Grant No. 25800238. GOURMET of the OCTA integrated simulation system (http://octa.jp) was used for data management. We thank Dr. E. Watters, Akita University, for English proofreading.

APPENDIX: AVERAGE TENSOR AROUND u_3

If the unit vectors $\boldsymbol{u}_1$ and $\boldsymbol{u}_2$ are randomly distributed around $\boldsymbol{u}_3$, one can get the following equations, where i stands for 1 or 2:

$$\langle \boldsymbol{u}_i \rangle_{\rm spin} = 0, \quad \langle \boldsymbol{u}_i \boldsymbol{u}_i \rangle_{\rm spin} = \tfrac{1}{2}(\boldsymbol{I} - \boldsymbol{u}_3\boldsymbol{u}_3), \quad \text{and } \langle \boldsymbol{u}_i \boldsymbol{u}_i \boldsymbol{u}_i \rangle_{\rm spin} = 0. \tag{A1}$$

Using the relation $\boldsymbol{u}_1 = \boldsymbol{u}_2 \times \boldsymbol{u}_3 = -\boldsymbol{u}_3 \times \boldsymbol{u}_2$, we have

$$\begin{aligned} \langle \boldsymbol{u}_1\boldsymbol{u}_2\boldsymbol{u}_3 \rangle_{\rm spin} &= \langle \boldsymbol{u}_1\boldsymbol{u}_2 \rangle_{\rm spin}\boldsymbol{u}_3 = -\boldsymbol{u}_3 \times \langle \boldsymbol{u}_2\boldsymbol{u}_2 \rangle_{\rm spin}\boldsymbol{u}_3 = -\boldsymbol{u}_3 \times \tfrac{1}{2}(\boldsymbol{I} - \boldsymbol{u}_3\boldsymbol{u}_3)\boldsymbol{u}_3 \\ &= -\tfrac{1}{2}\boldsymbol{u}_3 \times \boldsymbol{I}\boldsymbol{u}_3. \end{aligned} \tag{A2}$$

Using these equations for Eqs. (24)–(28), we have

$$\langle \boldsymbol{a} \rangle_{\rm spin} = \frac{3}{64\eta a}\left[\frac{1}{2}\left\{\frac{2a^2 + h^2(\cos^2(\theta/2) + 2)}{3h^2 + a^2(\sin^2(\theta/2) + 2)} + \frac{2a^2 + h^2(\sin^2(\theta/2) + 2)}{3h^2 + a^2(\cos^2(\theta/2) + 2)}\right\}(\boldsymbol{I} - \boldsymbol{u}_3\boldsymbol{u}_3) + \boldsymbol{u}_3\boldsymbol{u}_3\right], \tag{A3}$$

$$\langle \boldsymbol{b} \rangle_{\rm spin} = \frac{3}{64\eta a}\frac{h\sin\theta}{4}\left\{\frac{-1}{3h^2 + a^2(\sin^2(\theta/2) + 2)} + \frac{1}{3h^2 + a^2(\cos^2(\theta/2) + 2)}\right\}(\boldsymbol{I} - \boldsymbol{u}_3\boldsymbol{u}_3), \tag{A4}$$

$$\begin{aligned} \langle \boldsymbol{c} \rangle_{\rm spin} = \frac{3}{64\eta a}\Bigg[&\frac{1}{2}\left\{\frac{2 + \sin^2(\theta/2)}{3h^2 + a^2(\sin^2(\theta/2) + 2)} + \frac{2 + \cos^2(\theta/2)}{3h^2 + a^2(\cos^2(\theta/2) + 2)}\right\} \\ &\times (\boldsymbol{I} - \boldsymbol{u}_3\boldsymbol{u}_3) + \frac{1}{a^2}\boldsymbol{u}_3\boldsymbol{u}_3\Bigg], \end{aligned} \tag{A5}$$

$$\langle \tilde{g} \rangle_{{\rm spin},ijk} = g_{\rm spin}(e_{ilj}u_{3l}u_{3k} + e_{ilk}u_{3l}u_{3j}), \tag{A6}$$

where

$$g_{\rm spin} = -\frac{a^2 h\sin\theta}{8}\left(\frac{\cos^2(\theta/2)}{3h^2 + a^2(2 + \sin^2(\theta/2))} - \frac{\sin^2(\theta/2)}{3h^2 + a^2(2 + \cos^2(\theta/2))}\right), \tag{A7}$$

and

$$\langle \tilde{h} \rangle_{{\rm spin},ijk} = h_{\rm spin}(e_{ilj}u_{3l}u_{3k} + e_{ilk}u_{3l}u_{3j}), \tag{A8}$$

where

$$h_{\rm spin} = \frac{1}{2}\left\{\frac{3h^2 + a^2\sin^2\theta(\cos^2(\theta/2) + 2)}{3h^2 + a^2(\cos^2(\theta/2) + 2)} + \frac{3h^2 + a^2\cos^2\theta(\sin^2(\theta/2) + 2)}{3h^2 + a^2(\sin^2(\theta/2) + 2)}\right\}. \tag{A9}$$

For $a/h \ll 1$, we can expand the right-hand side of these equations with respect to a/h. Retaining the leading order terms in a/h, we have Eqs. (31)–(35).

[1] A. B. Harris, R. D. Kamien, and T. C. Lubensky, Molecular chirality and chiral parameters, Rev. Mod. Phys. **71**, 1745 (1999).

[2] M. Doi and M. Makino, Motion of microparticles of complex shape, Prog. Polym. Sci. **30**, 876 (2005).

[3] M. Makino and M. Doi, Migration of twisted ribbon-like particles in simple shear flow, Phys. Fluids **17**, 103605 (2005).

[4] N. Baranova and B. Y. Zel'dovich, Separation of mirror isomeric molecules by radio-frequency electric field of rotating polarization, Chem. Phys. Lett. **57**, 435 (1978).

[5] J. B. Clemens, O. Kibar, and M. Chachisvilis, A molecular propeller effect for chiral separation and analysis, Nat. Commun. **6**, 7868 (2015).

[6] M. Makino and M. Doi, Separation of chiral particles in a rotating electric field, Phys. Fluids **28**, 093302 (2016).
[7] J. Happel and H. Brenner, *Low Reynolds Number Hydrodynamics* (M. Nijhoff, Boston, 1983).
[8] S. Kim and S. Karrila, *Microhydrodynamics* (Butterworth-Heinemann, London, 1991).
[9] N. W. Krapf, T. A. Witten, and N. C. Keim, Chiral sedimentation of extended objects in viscous media, Phys. Rev. E **79**, 056307 (2009).
[10] B. Moths and T. A. Witten, Full Alignment of Colloidal Objects by Programed Forcing, Phys. Rev. Lett. **110**, 028301 (2013).
[11] B. Moths and T. A. Witten, Orientational ordering of colloidal dispersions by application of time-dependent external forces, Phys. Rev. E **88**, 022307 (2013).
[12] M. Makino and M. Doi, Brownian motion of a particle of general shape in Newtonian fluid, J. Phys. Soc. Jpn. **73**, 2739 (2004).
[13] D. L. Ermak and J. A. McCammon, Brownian dynamics with hydrodynamic interactions, J. Chem. Phys. **69**, 1352 (1978).
[14] M. P. Allen and D. Tildesley, *Computer Simulation of Liquids* (Clarendon Press, Oxford, U.K., 1986).
[15] H. Brenner, Rheology of a dilute suspension of axisymmetric Brownian particles, Int. J. Multiphase Flow **1**, 195 (1974).